ARTICLE

OPEN

Check for updates

Band transport evidence in PEDOT:PSS films using broadband optical spectroscopy from terahertz to ultraviolet region

Zijing Guo[1,5], Tetsu Sato[1,5], Yang Han[1], Naoki Takamura[1], Ryohei Ikeda[1], Tatsuya Miyamoto [1], Noriaki Kida[1], Makiko Ogino[2], Youtarou Takahashi [2], Naotaka Kasuya [1], Shun Watanabe [1], Jun Takeya [1,3], Qingshuo Wei [4], Masakazu Mukaida[4] & Hiroshi Okamoto [1,4✉]

Poly(3,4-ethylenedioxythiophene):poly(styrene sulfonate) (PEDOT:PSS) is a prototypical conducting polymer. When a polar solvent is used during film fabrication, the hole-doped PEDOT oligomers form crystalline clusters in the films, exhibiting high conductivity. However, whether hole carriers exhibit band transport has not been clarified yet. Here, we employ a multilayer spin-coating method using an aqueous solution with ethylene glycol, with additional procedures of dipping the films in ethylene glycol or dropping sulfuric acid onto the films, to achieve a high DC conductivity of $\sim 1000\,S\,cm^{-1}$ or higher. Using terahertz time-domain spectroscopy and far-infrared-to-ultraviolet reflection spectroscopy, we derive complex optical conductivity $\tilde{\sigma}$ spectra, which are reproduced by the sum of the Drude response, and Lorentz-oscillator responses due to phonons. These results demonstrate the band transport, which is further confirmed by the Hall effect measurements. The hole mobility estimated from the spectral analyses is 7–$11\,cm^2\,V^{-1}\,s^{-1}$, a significantly large value. The reported evaluation methods for broadband $\tilde{\sigma}$ spectra can help elucidate carrier transport mechanisms in various conducting films.

[1] Department of Advanced Materials Science, University of Tokyo, Kashiwa, Chiba 277-8561, Japan. [2] Department of Applied Physics and Quantum Phase Electronics Center, University of Tokyo, Tokyo 113-8656, Japan. [3] International Center of Materials Nanoarchitectonics (WPI-MANA), National Institute for Materials Science (NIMS), 1-1 Namiki, Tsukuba 305-0044, Japan. [4] National Institute of Advanced Industrial Science and Technology (AIST)-University of Tokyo Advanced Operando-Measurement Technology Open Innovation Laboratory (OPERANDO-OIL), AIST, 5-1-5 Kashiwanoha, Kashiwa, Chiba 277-8589, Japan. [5] These authors contributed equally: Zijing Guo, Tetsu Sato. ✉email: okamotoh@k.u-tokyo.ac.jp

Transparent and conducting thin films can be applied as transparent electrodes in wearable devices and as hole-transport layers in solar cells[1–3]. For such films, organic polymers have advantages over existing inorganic metal materials, such as their ability to be fabricated by solution processes, ease of large-area production, light weight, and flexibility. Furthermore, they are cost-effective and do not contain rare metals, which corresponds with current resource strategies, making them promising next-generation electronic materials[2,4–9]. In organic polymers with π-conjugated systems, high DC conductivity has been achieved by chemical carrier doping[10–17], utilising the redox properties of the constituent molecules[18,19]; moreover, control over the doping level via electrochemical methods has been reported[20–24].

Poly(3,4-ethylenedioxythiophene): poly(styrenesulfonate) (PEDOT:PSS) is a well-known polymer that exhibits high DC conductivity through chemical carrier doping in its films (Fig. 1a). In those films, it has been established that holes are doped via electron transfer during the oxidative polymerisation of PEDOT, an oligomer of the EDOT molecule[25–27]. PSS is used to stabilise the doped PEDOT molecules and achieve charge equilibrium. Reportedly, doped PEDOT molecules form clusters, and macroscopic DC conductivity occurs via the transfer of hole carriers between these clusters. Typically, PEDOT oligomers and insulating PSS long-chain polymers complexed by electrostatic attractive forces assume a colloidal state, including a high concentration of neutral PSS[28,29]. In this state, the clusters of PEDOT oligomers are fragmented by PSS, and the transfer of hole carriers between the clusters is inhibited. Therefore, the DC conductivity of the PEDOT:PSS film remains in the order of 10^1 S cm^{-1} (left panel of Fig. 1b). In contrast, in PEDOT:PSS films fabricated by the addition of polar solvents such as ethylene glycol (EG) or dimethyl sulfoxide (DMSO), insulating PSS is more likely to be excluded. As confirmed by X-ray diffraction, X-ray photoelectron spectroscopy (XPS), and visible (Vis) spectroscopy[27,30–32], the PEDOT molecules are packed more closely to form clusters, as shown in the middle panel of Fig. 1b. Simultaneously, the insulating PSS, which hinders the transfer of hole carriers between clusters, also decreases[33]. These effects lead to a higher DC conductivity of ~500 S cm^{-1} [34]. Furthermore, neutral PSS molecules in the films thus obtained are reportedly further excluded by exposing the films to EG or by dropping sulfuric acid on them, resulting in high DC conductivity and high carrier mobility that exceed 1000 S cm^{-1} and 1 cm^2 V^{-1} s^{-1}, respectively[35–39] (the right panel of Fig. 1b). In particular, in the case of the sulfuric acid dropping procedure, the effect of PSS exclusion is accelerated by the protonation of PSS[38–40], resulting in a larger conductivity enhancement up to ~4000 S cm^{-1} [36,38]. More recently, an example has been reported in which the molecular weight was controlled by incorporating PEDOT side-chain interactions to promote crystallisation, again achieving a DC conductivity in excess of 1000 S cm^{-1} [40]. In such highly conductive films, the barriers to the transfer of holes between adjacent PEDOT clusters are expected to decrease, allowing holes to behave as free carriers and potentially exhibit band transport. However, no clear evidence of band transport has been obtained thus far.

An effective method for investigating carrier transport mechanisms is to measure complex optical conductivity ($\tilde{\sigma}$) spectra. In fact, for PEDOT:PSS films, $\tilde{\sigma}$ spectra in the frequency range of 0.1 THz to 3 THz were measured by applying terahertz time-domain spectroscopy (THz-TDS) on samples with the DC conductivity of ~500 S cm^{-1}, which were prepared from EG-added solutions[41]. However, the obtained spectra could not be explained using the Drude model, which expresses the low-frequency response of a simple metal. Instead, the aforementioned spectra were reproduced using the localisation-modified Drude (LMD) model[34,41], indicating that holes doped in PEDOT molecules do not behave as free carriers but are subject to localisation effects. In another study that applied THz-TDS to films formed from DMSO-added solutions, the $\tilde{\sigma}$ spectra obtained were again not reproduced by the simple Drude model but were analysed using the Drude-Smith model[42], which incorporates the effect of extrinsic backscattering of hole carriers[43,44]. Other spectroscopic studies ranging from the mid-infrared (MIR) to Vis region have also been conducted; however, they were limited to absorption and reflectivity measurements, with $\tilde{\sigma}$ spectra that can directly reflect the carrier transport mechanism not being derived from the obtained absorption and reflectivity spectra[31,38].
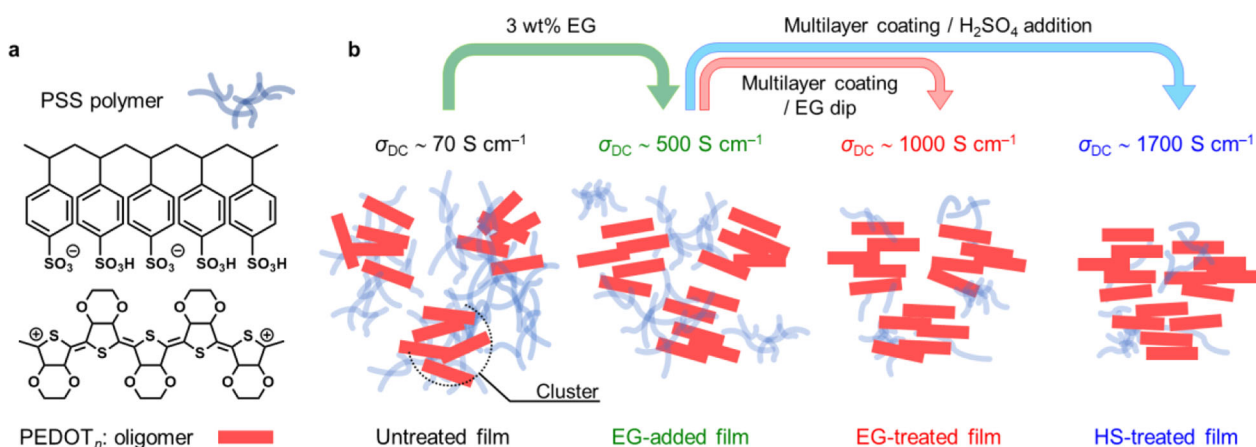

Fig. 1 Molecular structure and morphology of PEDOT:PSS. a Chemical structures of PEDOT oligomer and PSS polymer in PEDOT:PSS composite. **b** Schematic structures of PEDOT:PSS composite films prepared by the spin-coating method using aqueous dispersion of PEDOT:PSS. The leftmost panel shows the Untreated film, in which a lot of PSS molecules make difficult a close interaction between neighbouring PEDOT clusters. The second panel from left shows the EG-added film, in which by adding EG to the aqueous dispersion of PEDOT:PSS, PSS polymers are partially excluded and PEDOT oligomers tended to align in the film. It resulted in the increase of DC conductivity σ_{DC}. The third panel from left and rightmost panel show the EG-treated and HS-treated films, respectively, which are prepared by a multilayer spin-coating from the EG-added aqueous dispersion of PEDOT:PSS. After each spin-coating, the film is dipped to EG in the EG-treated film and H$_2$SO$_4$/methanol solution is drop-casted onto the film in the HS-treated film (see "Methods"). In these films, PSS polymers are further excluded and the resultant close molecular interactions between neighbouring PEDOT clusters further increase σ_{DC}.

Table 1 DC conductivity (σ_{DC}), σ_1 extrapolated to frequency zero (σ_0), carrier density (N) and carrier mobility (μ) in PEDOT:PSS films.

	HS-treated film	EG-treated film	EG-added film	Untreated film
σ_{DC} (S cm^{-1})	~1620	~950	~500	~70
σ_0 (S cm^{-1})	1680	980	500	245
N (10^{20} cm^{-3})	9.4 ± 0.2	8.4 ± 0.2	7.5 ± 0.2	6.1 ± 0.2
μ (cm^2 V^{-1} s^{-1})	10.7 ± 0.3	7.1 ± 0.2	4.1 ± 0.1	0.71 ± 0.02

Based on the aforementioned background, this study aims to spectroscopically elucidate the carrier transport mechanism in highly conducting PEDOT:PSS films, specifically, whether holes doped in PEDOT molecules undergo band transport or are subject to localisation effects owing to possible molecular disorders[45]. The PEDOT:PSS film samples are fabricated using a multilayer spin-coating method with a water-based solution containing EG, and their DC conductivities are further enhanced by dipping the films in EG or dropwise addition of sulfuric acid to the films. The DC conductivities of the films treated by dipping in EG and dropwise addition of sulfuric acid are ~1000 S cm^{-1} and 1700 S cm^{-1}, respectively. A unique technique combining THz-TDS and far-infrared (FIR) to ultraviolet (UV) reflection spectroscopy is applied to the samples to derive accurate $\tilde{\sigma}$ spectra ranging from THz to UV region. The obtained spectra are reproduced by the sum of the Drude response owing to hole carriers and the Lorentzian responses owing to phonons. These results demonstrate the band transport of hole carriers, which is further supported by Hall effect measurements.

Results

Sample preparations and DC conductivity measurements.

Four types of PEDOT:PSS films are prepared using a spin-coating method involving an aqueous dispersion of PEDOT:PSS, and the DC conductivity σ_{DC} of each film is measured using a four-point probe method[36]. First, a 100-nm-thick film is fabricated via PEDOT:PSS aqueous dispersion with 3 wt% EG using a single spin-coating process. Moreover, σ_{DC} is ~500 S cm^{-1}. This sample is referred to as the EG-added film.

By performing multiple spin-coating processes (multilayer spin-coating method), σ_{DC} increases to ~850 S cm^{-1}. The film is then dipped in EG and removed, yielding a film with a thickness of 800 nm. Through this EG dipping process, σ_{DC} increases to ~950 S cm^{-1}. This film is referred to as the EG-treated film.

To obtain a higher DC conductivity, sulfuric acid drop treatment[36,37], a known method to increase conductivity, is performed for each spin-coating process that involves PEDOT:PSS aqueous dispersion with added EG. This process is repeated several times to produce a film with a thickness of 800 nm. The resulting film, referred to as the HS-treated film, exhibits a σ_{DC} value of ~1620 S cm^{-1}.

As a reference for the two highly conductive samples, a film with a thickness of 800 nm is fabricated via an EG-free aqueous dispersion of PEDOT:PSS using a multilayer spin-coating method. This film is hereafter referred to as the Untreated film. Furthermore, σ_{DC} of this film is ~70 S cm^{-1}.

The fabrication methods for these films are described in detail in the Methods section. Moreover, σ_{DC} values of each sample at 294 K are listed in Table 1. No directional dependence exists in σ_{DC}. Compared to the Untreated film (σ_{DC}~70 S cm^{-1}), the EG-added film, EG-treated film, and HS-treated film exhibit σ_{DC} values that are approximately sevenfold (σ_{DC}~500 S cm^{-1}), 14-

fold (σ_{DC}~950 S cm^{-1}), and 23-fold (σ_{DC}~1620 S cm^{-1}) higher, respectively. The relative increases in σ_{DC} for these three types of films align well with those of previously reported films fabricated using similar methods[41,46,47].

THz time-domain spectroscopy.

First, THz-TDS is applied to the four types of PEDOT:PSS films to evaluate the complex optical conductivity $\tilde{\sigma}(\omega) = \sigma_1(\omega) + i\sigma_2(\omega)$ in the frequency range of 0.75–2.6 THz. Hereafter, $\tilde{\sigma}(\omega)$, $\sigma_1(\omega)$ and $\sigma_2(\omega)$ are simply expressed as $\tilde{\sigma}$, σ_1 and σ_2, respectively. This frequency range corresponds to the region in which the response of the carriers to the oscillating electric field becomes prominent. THz-TDS allows for direct measurement of $\tilde{\sigma}$. The frequency dependence (spectrum) of $\tilde{\sigma}$ provides information on the carrier transport mechanism, such as the scattering probability and localisation effect of carriers, which cannot be obtained through DC conductivity or carrier mobility measurements alone[45,48–50]. THz-TDS is further detailed in "Methods".

Figure 2a–d shows the spectra of the real part (σ_1) and imaginary part (σ_2) of $\tilde{\sigma}$ for the four types of samples. In the Untreated film and EG-added film, σ_1 decreases towards lower frequencies. The values of σ_1 extrapolated to frequency zero, denoted as σ_0, are 245 S cm^{-1} and 500 S cm^{-1} for the Untreated and EG-added films, respectively. The σ_0 value for the EG-added film matches well with the DC conductivity (σ_{DC}) of ~500 S cm^{-1}. The σ_0 value for the Untreated film is larger than σ_{DC} of ~70 S cm^{-1}, which is due to the poor extrapolation caused by strong carrier localisation (see Supplementary Note 1). In contrast, the σ_1 values for the EG- and HS-treated films show almost no frequency dependence within the measurement range and remain nearly constant at 980 S cm^{-1} and 1680 S cm^{-1}, respectively. These values closely match the corresponding σ_{DC} values (950 S cm^{-1} and 1620 S cm^{-1} in EG- and HS-treated films, respectively). These results demonstrate that the optical conductivity (σ_1) measured by THz-TDS effectively reflects the macroscopic transport characteristics (σ_{DC}) due to hole carriers.

In the Untreated and EG-added films, with decreasing frequency, σ_1 decreases as mentioned above, while σ_2 takes negative values and increases towards zero. For samples prepared using methods similar to those herein for these two films, $\tilde{\sigma}$ spectra in the same frequency range have been previously reported[41]. The shapes of the $\tilde{\sigma}$ spectra obtained in this study qualitatively agree with theirs. As mentioned earlier, in a previous report, both of the σ_1 and σ_2 spectra were almost reproduced using the LMD model, which incorporates backscattering of carriers at barriers between highly conductive clusters or domains. The decrease in σ_1 and increase in σ_2 with decreasing frequency are interpreted as the results of carrier localisations. Furthermore, as summarised in Table 1, the σ_{DC} value of the EG-added film is larger than that of the Untreated film, and the decrease (increase) in σ_1 (σ_2) for lower frequencies in the former is smaller than that in the latter. These trends are consistent with those observed in previous studies[41]. These results indicate that the addition of EG reduces the effect of carrier localisation.

In contrast, in the EG- and HS-treated films, which exhibit high σ_{DC}, σ_1 is almost constant below 2.5 THz (Fig. 2c, d). This behaviour is characteristic of a simple metal, as described by the Drude model and suggests that the carrier localisation effect is significantly weak in both films. As mentioned earlier, when the carriers are localised, σ_2 becomes negative at low frequencies. Although the values of σ_2 in these two films are slightly negative, their absolute values are extremely small, which is consistent with the absence of significant carrier localisation. The origin of negative σ_2 is discussed in more detail later in this paper. The fact that σ_1 is constant and σ_2 is relatively small implies that the
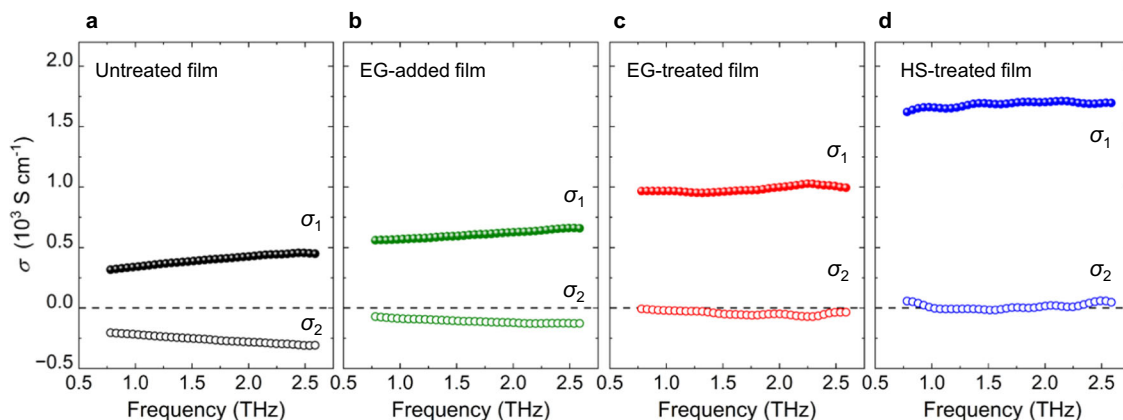
Fig. 2 Spectra of complex optical conductivity ($\widetilde{\sigma}$) in the THz region in four types of PEDOT:PSS films. a Untreated film, **b** EG-added film, **c** EG-treated film, and **d** HS-treated film (see the text).

damping constant reflecting the carrier scattering rate, γ, is in a frequency range significantly higher than the measured region.

Broadband optical reflectivity and complex optical conductivity spectra. To obtain quantitative information on the carrier transport mechanism from the $\widetilde{\sigma}$ spectra, the spectra must be measured not only in the THz region but also in a higher-frequency region ranging from the FIR to the UV region. In this high-frequency region, obtaining $\widetilde{\sigma}$ spectra directly is difficult because TDS cannot be performed. In this study, the optical reflectivity (R) spectrum is measured for EG- and HS-treated films. By connecting the R spectrum in this region with that calculated from the $\widetilde{\sigma}$ spectrum in the THz region, a broadband R spectrum is obtained, which can be converted to the $\widetilde{\sigma}$ spectrum using the Kramers–Kronig transform (KKT).

The R spectrum in the THz region is calculated from the $\widetilde{\sigma}$ spectrum using the following equations,

$$\frac{\widetilde{\varepsilon}(\omega)}{\varepsilon_0} = 1 + \frac{i\widetilde{\sigma}(\omega)}{\omega\varepsilon_0},$$

$$\varepsilon_1(\omega) = \varepsilon_0 - \frac{\sigma_2(\omega)}{\omega}, \quad \varepsilon_2(\omega) = \frac{\sigma_1(\omega)}{\omega}, \tag{1}$$

and

$$R(\omega) = \left| \frac{\left(\frac{\widetilde{\varepsilon}(\omega)}{\varepsilon_0}\right)^{\frac{1}{2}} - 1}{\left(\frac{\widetilde{\varepsilon}(\omega)}{\varepsilon_0}\right)^{\frac{1}{2}} + 1} \right|^2, \tag{2}$$

where $\widetilde{\varepsilon}(\omega) = \varepsilon_1(\omega) + i\varepsilon_2(\omega)$ is the complex dielectric constant and ε_0 is the vacuum dielectric constant. Hereafter, $\widetilde{\varepsilon}(\omega)$, $\varepsilon_1(\omega)$, and $\varepsilon_2(\omega)$ are simply expressed as $\widetilde{\varepsilon}$, ε_1 and ε_2, respectively.

For the measurement of R spectrum on the higher-frequency side, Fourier transform infrared spectroscopy (FTIR) is used in both the FIR region (0.012–0.08 eV) and the MIR region (0.08–0.5 eV). In the UV–Vis region (0.5–6 eV), a diffraction grating spectrometer is used. The overall R spectra of the EG- and HS-treated films are shown in Fig. 3. Further details of the measurements are provided in "Methods".

With decreasing photon energy in the Vis region, the R spectrum of the EG-treated film (Fig. 3a) exhibits a sharp increase around 1.05 eV, as indicated by the dashed line in Fig. 3c. It shows fine peak structures in the range of 0.05–0.2 eV and then gradually increases further. The enlarged view of the fine structures ranging from 0.05 to 0.2 eV is shown in Fig. 3d as a

red line. Note that the sharp infrared vibrations, indicated by thin vertical lines, are superimposed on the broad electronic response.

In the R spectrum of the HS-treated sample (Fig. 3b), R rises at 1.15 eV, as indicated by the dashed line in Fig. 3c, which is slightly higher than that of the EG-treated film. However, the overall shape of the R spectrum is similar to that of the EG-treated film. In addition, the vibrational structures indicated by the blue line in Fig. 3d are very similar to those of the EG-treated film. Therefore, both the shape of the structure due to the broad electronic response (Fig. 3b) and the vibrational structures due to the sharp infrared vibrations (Fig. 3d) exhibit similar tendencies as those of the EG-treated film. The R value at the lower energy bound of the measured region, ~3 meV (0.7 THz), exceeds 95% for both films. Based on these results, the R spectra of the two films can be attributed to a combination of the Drude response characteristics of the metals and the structures caused by infrared-active phonons.

Previous studies on the vibrational modes in PEDOT molecules doped with hole carriers by electrochemical methods[51–53] have provided important information about the origin of the sharp vibrational structures depicted in Fig. 3d. According to these studies, the vibrational structures in this frequency region are primarily attributed to the doped PEDOT molecular backbone. Moreover, the frequencies and intensities of these vibrational modes reportedly depend on doping concentration. In Fig. 3d, the peak frequencies of the vibrational structures in the EG-treated- and HS-treated films are in good agreement, as indicated by the vertical thin lines. Furthermore, these peak positions align with those of the vibrational structures observed in the Untreated film (see Supplementary Note 2). These results suggest that the number of holes per molecule remains unchanged regardless of the fabrication method of the PEDOT:PSS films. This finding is consistent with previous studies indicating that the X-ray photoelectron spectra specific to the S atoms in the PEDOT molecular backbone do not shift due to polar solvent treatments[27,54,55].

To obtain more detailed information from the R spectra, the broadband $\widetilde{\sigma}$ spectra of the EG- and HS-treated films are obtained using KKT. The results are indicated by the solid black lines in Fig. 4a–d. In the THz region, the $\widetilde{\sigma}$ spectra are directly obtained using THz-TDS, as represented by the green open circles. The $\widetilde{\sigma}$ spectra obtained by KKT adequately reproduce the $\widetilde{\sigma}$ spectra calculated directly from THz-TDS (open circles). This confirms the high accuracy of KKT. In both films, as the photon energy decreases from the high-energy side, σ_1 increases around 1 eV, exhibits peaks due to vibrational structures, and then shows a flat spectrum (Fig. 4a, c). In contrast, σ_2 is
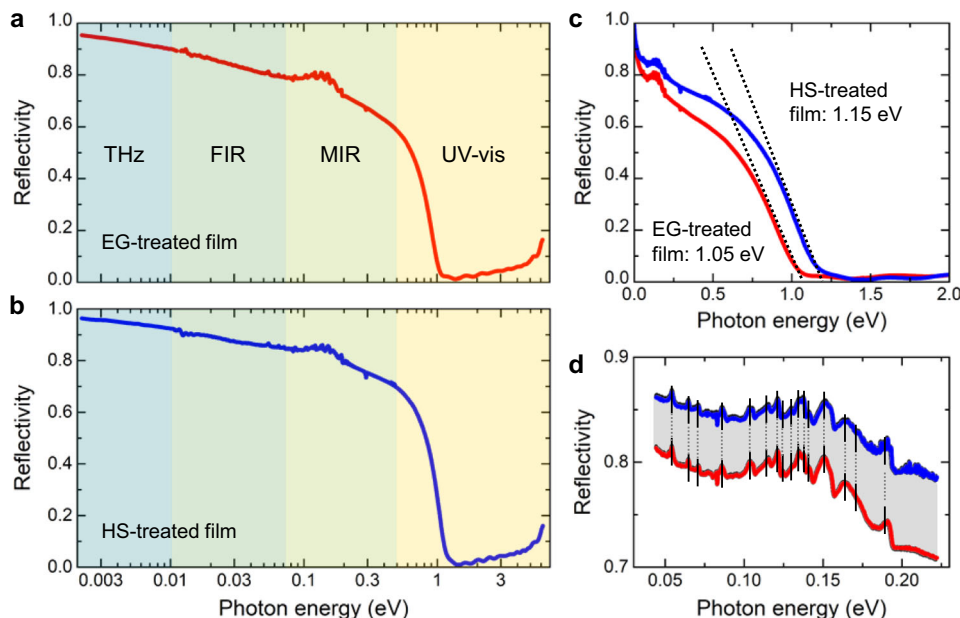
Fig. 3 Broadband optical reflectivitiy (R) spectra in the EG-treated film and HS-treated film. a, b Overall R spectra with the horizontal axis on logarithmic scale. The spectra in different-coloured areas were measured using different spectroscopy methods: THz, FIR, MIR and UV–Vis means THz-TDS, Fourier transform FIR spectroscopy, Fourier transform MIR spectroscopy, and UV to Vis spectroscopy, respectively. **c** Overall spectra with the horizontal axis on linear scale. The point where each dotted line intersects the horizontal axis indicates the photon energy at which the metallic reflection band rises. This energy is slightly higher in the HS-treated film than in the EG-treated film. **d** Expanded R spectra from 0.04 eV to 0.22 eV. The vertical black lines show the peak structures due to phonons, the energy positions of which are almost the same in the two films (also see Supplementary Notes 2 and 4).
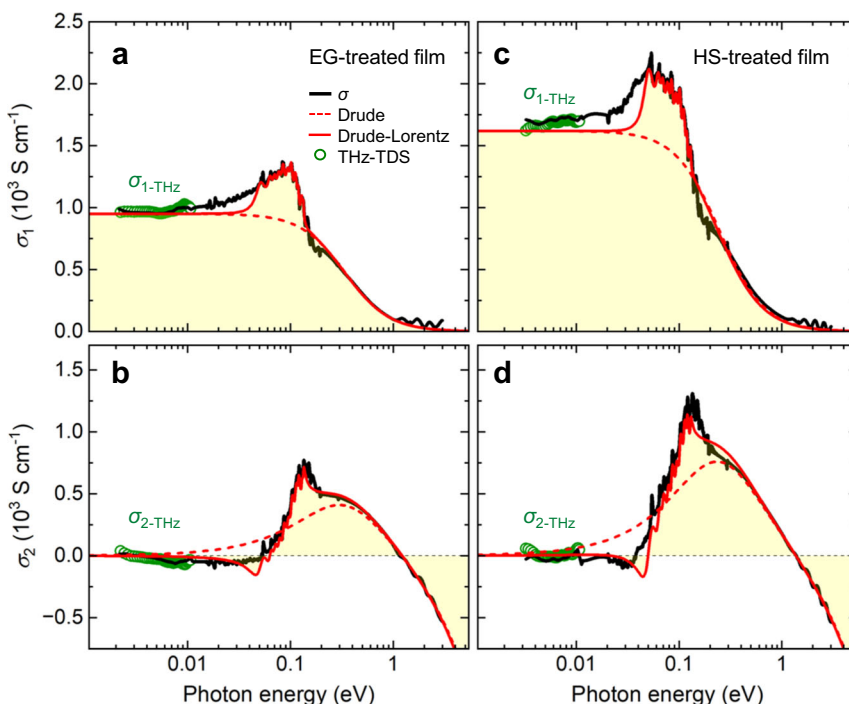

Fig. 4 Broadband complex optical conductivity ($\widetilde{\sigma}$) spectra in the EG-treated film and HS-treated film. a–d Real part σ_1 (**a**, **c**) and imaginary part σ_2 of $\widetilde{\sigma}$ (**b**, **d**, black lines) obtained from the KKT of R spectra in Fig. 3a, b. σ_1 and σ_2 spectra in the THz region are in good agreement with the spectra (green open circles) denoted by $\sigma_{1\text{-THz}}$ and $\sigma_{2\text{-THz}}$, which were directly obtained by THz-TDS. The red broken and solid lines show the fitting curves obtained using the simple Drude model and Drude–Lorentz model, respectively.

negative in the high-energy region and monotonically increases, becoming positive around 1 eV. Then, it saturates around 0.3 eV, exhibiting peaks due to phonon structures. It becomes slightly negative near 0.04 eV, and finally approaches zero (Fig. 4b, d).

Evaluations of carrier density in each film. To evaluate the physical parameters dominating the carrier transport by the analyses of the $\widetilde{\sigma}$ spectra, it is effective to estimate the carrier density of each film. In PEDOT:PSS films fabricated via a spin-coating method using a PEDOT:PSS dispersion aqueous solution,

it is known that the original ratio of PEDOT and PSS in the aqueous solution is preserved[56]. Therefore, the mass ratio (w/w) of PEDOT:PSS in the Untreated film can be considered as 1/2.5. In addition, the weight densities per unit volume of PEDOT and PSS are almost identical to each other, being almost equal to 1.5 g cm^{-3} (see ref. [56]). In the other films, the weight density per unit volume in a PEDOT:PSS film may be changed by an addition of EG. To measure the change in the weight density per unit volume in a PEDOT:PSS film by an addition of EG, an EG-added film with a thickness of ~30 μm was prepared on a glass substrate using a 3 wt% EG-doped PEDOT:PSS solution via the spin-coating method, and the film is then peeled off from the substrate. From the volume and weight of the freestanding film, the weight density of PEDOT:PSS in the EG-added film is evaluated as ~1.5 g cm^{-3}. Since the weight densities of PEDOT and PSS are almost identical as mentioned above, it is reasonable to consider that the weight density is still equal to 1.5 g cm^{-3} in the EG- and HS-treated films obtained after the additional treatments as well as in the EG-added film.

The mass ratio of PEDOT in the PEDOT:PSS films is likely to be changed from 1/2.5 in the EG-added, EG-treated, and HS-treated films due to the reductions of PSS. From the absorption intensity specific to PSS in the UV–Vis region, the mass ratio of PEDOT:PSS, w/w, is evaluated as ~1/1.85 in the EG-added film, 1/1.57 in the EG-treated film, and 1/1.28 in the HS-treated film (see Supplementary Note 3 and Fig. 3). The previous studies have revealed that the hole density per EDOT, N_{EDOT}, is ~1/3[57–59]. Furthermore, the analyses of the vibrational structures in the optical spectra mentioned earlier show that N_{EDOT} is unchanged by the EG and sulfuric acid treatments, suggesting that N_{EDOT} is still ~1/3. Using these mass ratios of PEDOT:PSS and the relation $N_{EDOT} = 1/3$, the hole carrier density is estimated to be 6.1×10^{20} cm^{-3} in the Untreated film, 7.5×10^{20} cm^{-3} in the EG-added film, 8.4×10^{20} cm^{-3} in the EG-treated film, and 9.4×10^{20} cm^{-3} in the HS-treated film, which are listed in Table 1.

The estimated change in N can be reasonably explained as follows. When more neutral PSS polymers are excluded from a PEDOT:PSS film, the density of the PEDOT oligomers increases, while the hole density in the PEDOT oligomer remains unchanged, which enhances the hole density per unit volume. HS or EG treatment leads to a decrease in the film thickness owing to the exclusion effect of neutral PSS polymers[32,60–62]. In this study, the film thickness is measured after HS or EG treatment, and the rotation speed of the substrate in each spin-coating process is adjusted to achieve a final thickness of 800 nm for both films. Compared with the EG treatment, the exclusion of neutral PSS is easier in the HS treatment; therefore, the density of PEDOT should increase after the HS treatment, resulting in an apparent increase in N in the HS-treated film.

Analyses of broadband complex optical conductivity spectra in EG-treated and HS-treated films. To elucidate the origins of these spectral shapes in the highly conductive EG-treated and HS-treated films, an analysis is performed using a simple Drude model. The $\widetilde{\sigma}$ spectra deduced using the Drude model are given by the following equation.

$$\widetilde{\sigma} = \frac{\omega}{i}\left[(\varepsilon_\infty - \varepsilon_0) - \frac{Ne^2}{m^*}\frac{1}{\omega^2 + i\gamma\omega}\right]$$
$$\sigma_1 = \frac{Ne^2}{m^*}\frac{\gamma}{\omega^2 + \gamma^2}, \quad \sigma_2 = (\varepsilon_0 - \varepsilon_\infty)\omega + \frac{Ne^2}{m^*}\frac{\omega}{\omega^2 + \gamma^2}$$

(3)

Here, m^* is the effective mass of the hole carriers, e is the elementary charge, γ is the damping constant, and ε_∞ is the high-frequency dielectric constant. The plasma frequency ω_p characterising the Drude response is defined as follows.

$$\omega_p = \left(\frac{Ne^2}{\varepsilon_\infty m^*}\right)^{\frac{1}{2}}$$

(4)

Equation (3) is used to fit the portion of the experimentally obtained $\widetilde{\sigma}$ spectra excluding the vibrational structures in the range of 0.01–0.2 eV. The fitting parameters are m^*, γ and ε_∞. As mentioned above, in the films investigated here, the extrapolated values of σ_1 to the frequency zero, σ_1 (0), are consistent with $\sigma_{DC} = 950$ S cm^{-1}. Therefore, it is effective to perform the fitting so that σ_1 (0) should be equal to σ_{DC}. Since $\sigma_1(0) = \frac{Ne^2}{m^*\gamma}$ obtained from Eq. (3) shows that the product of m^* and γ is constant, the fitting parameters can be reduced to two, γ and ε_∞.

The red dashed lines in Fig. 4a–d show the fitting curves, which generally reproduce the broad structures in both σ_1 and σ_2 spectra in both the EG-treated and HS-treated films. The used parameter values of γ and ε_∞ are listed in Table 2. The additional parameters m^* and ω_p are calculated from those parameters and experimentally obtained N and σ_{DC} as listed in Table 2.

In contrast, in the energy region (0.15–0.3 eV), including the vibrational structures, σ_1 shows a shaved depression and is lower than the fitting curve with the Drude model. This is attributed to Fano interference that occurs due to the interaction between phonons and conduction carriers[63,64]. Therefore, among the infrared vibrational structures indicated by the thin lines in Fig. 3d, only the structures of 11(10) infrared vibrations on the low-energy side for the EG-treated (HS-treated) film, where the effect of Fano interference is relatively small, are included as Lorentz oscillators. Next, the $\widetilde{\sigma}$ spectra are attempted to fit using the Drude–Lorentz model, as expressed by the following equation, in which these oscillators are added to the Drude component in response (Eq. (3)).

$$\widetilde{\sigma} = \frac{\omega}{i}\left[(\varepsilon_\infty - \varepsilon_0) - \frac{Ne^2}{m^*}\frac{1}{\omega^2 + i\gamma\omega} + \varepsilon_0\sum_j\frac{f_j}{\omega_j^2 - \omega^2 - i\Gamma_j\omega}\right]$$

(5)

Table 2 Physical parameters in PEDOT:PSS films.

	Model	$\frac{m^*}{m_0}$	$\hbar\gamma$ (eV)	$\frac{C}{(k_F v_F)^2}$ (fs^2)	$\frac{\varepsilon_\infty}{\varepsilon_0}$	$\hbar\omega_p$ (eV)
Untreated film	LMD	0.564 ± 0.021	0.189 ± 0.007	11.4 ± 0.9	2.59 ± 0.01	0.760 ± 0.016
EG-added film	LMD	0.52 ± 0.02	0.288 ± 0.009	2.43 ± 0.14	2.59 ± 0.01	0.878 ± 0.018
EG-treated film	Drude	0.481 ± 0.014	0.341 ± 0.009	—	2.54 ± 0.03	0.972 ± 0.024
	Drude–Lorentz	0.487 ± 0.005	0.336 ± 0.004	—	2.59 ± 0.01	0.958 ± 0.007
HS-treated film	Drude	0.435 ± 0.011	0.249 ± 0.007	—	2.56 ± 0.05	1.08 ± 0.03
	Drude–Lorentz	0.453 ± 0.006	0.238 ± 0.003	—	2.60 ± 0.02	1.05 ± 0.01

Errors indicate the standard deviation of the least squares fit. m^* in the EG-added film is set to $0.52m_0 \pm 0.02m_0$ (see the text). Errors of ε_∞ in the Untreated and EG-added films are assumed to be the same as those estimated in the EG-treated film.

Here, ω_j, Γ_j, and f_j are the frequency, damping constant, and oscillator strength of each phonon, respectively. The fitting parameters of this analysis are γ and ε_∞, which are used for the analysis with the Drude model mentioned above, as well as the parameters ω_j, Γ_j, and f_j associated with each phonon. The fitting results are shown by the red solid lines in Fig. 4a–d with the yellow shadings, which adequately reproduce the σ_1 and σ_2 spectra simultaneously in both films. The R spectra calculated using these fitting parameters are also verified to closely replicate the experimental R spectra (Supplementary Note 4 and Fig. 4). In Fig. 2c, d, it is noted earlier that the σ_2 values in the terahertz region are slightly negative. These negative values of σ_2 cannot be reproduced by the Drude model alone but can be almost reproduced by assuming Lorentz oscillators for the fitting of the phonon structures.

The obtained parameters of $\hbar\gamma \sim 0.34$ eV in the EG-treated film and $\hbar\gamma \sim 0.24$ eV in the HS-treated film leads to $m^* \sim 0.49 m_0$ and $0.45 m_0$, respectively. The mobility values of hole carriers, μ, can be estimated from σ_{DC} and N values as 7.1 cm^2 V^{-1} s^{-1} and 10.7 cm^2 V^{-1} s^{-1} for the EG- and HS-treated films, respectively, which are listed in Table 1. These values of μ are higher than those previously reported in conducting PEDOT:PSS films[32,46,65,66] and consistent with the observed band transport features. Considering the relation $\mu = e/(m^*\gamma)$, the high mobility values are considered to originate from the small values of m^* and γ. The precise parameter values of $\hbar\gamma$, m^*, ε_∞ and $\hbar\omega_p$ obtained by these Drude–Lorentz model analyses are also listed in Table 2. The parameters related to the vibrational structures are reported in Supplementary Note 5.

The values of γ, ε_∞ and m^* obtained from the Drude and Drude–Lorentz model analyses are consistent with each other in each film. No significant differences exist in the vibrational parameters of the EG- and HS-treated films (Supplementary Note 5). In particular, the frequencies of each vibrational mode of the two films match well. Thus, based on the reproduction of the electronic response reflected by the broad components of the $\widetilde{\sigma}$ spectra by the simple Drude model, band transport of hole carriers is evident in these PEDOT:PSS films.

Herein, the parameters obtained by applying the Drude–Lorentz model to the $\widetilde{\sigma}$ spectra in the EG- and HS-treated films are further compared (Table 2). The high-frequency dielectric constant $\varepsilon_\infty/\varepsilon_0$ equals 2.59 and 2.60 for the EG- and HS-treated films, respectively. These values are typical for low-dielectric organic polymers and almost consistent with those previously reported for PEDOT:PSS films[41]. The essential differences between the EG-treated and HS-treated films manifest themselves in the relative decreases in γ and m^* in the HS-treated film, which are responsible for the increase in mobility μ as pointed out above. m^* discussed here characterises the sample-dependent effective band shape, reflecting carrier transfers between neighbouring PEDOT clusters, and it is reasonable to assume that γ also strongly depends on the scattering of carriers as they move between neighbouring PEDOT clusters. In other words, our study clearly demonstrates that in the HS-treated film the relative decrease in PSS polymers which are obstacles to the carrier transport causes the decreases in both γ and m^* via the enhancement of the carrier transfer probability between neighbouring PEDOT clusters and finally leads to the enhancement of the mobility μ.

Until now, the $\widetilde{\sigma}$ spectra of PEDOT:PSS films have only been evaluated in the THz region. Spectroscopic studies in the higher-frequency region have been limited to reflectivity or absorption measurements, making it difficult to derive $\widetilde{\sigma}$ spectra and preventing detailed analyses of electronic responses that reflect carrier dynamics. In related studies that derive $\widetilde{\sigma}$ spectra,

spectroscopic ellipsometry has been applied to PEDOT:Tos films with tosylate (Tos) ions as counterions[67,68]. However, even in these studies, the obtained spectral range of $\widetilde{\sigma}$ is limited, and no metallic response is observed. This study accurately evaluates the broadband $\widetilde{\sigma}$ spectra, successfully demonstrating a metallic response following a simple Drude model in highly conducting PEDOT:PSS films.

Analyses of terahertz complex optical conductivity spectra in Untreated and EG-added films. In the Untreated and EG-added films, the $\widetilde{\sigma}$ spectra in the terahertz region cannot be reproduced by the simple Drude model: σ_1 decreases towards frequency 0 and σ_2 takes negative values in the low-frequency region (see Fig. 2). In fact, their μ values estimated from σ_{DC} and N, 0.71 cm^2 V^{-1} s^{-1} in the Untreated film and 4.1 cm^2 V^{-1} s^{-1} in the EG-added film, are smaller than those in EG- and HS-treated films as shown in Table 1. These results suggest that all carriers are subject to finite localisation effects even at room temperature. To analyse such spectra, the LMD model was used in the previous study[41], in which an Untreated film with σ_{DC} of 7.6 S cm^{-1} and an EG-added film with σ_{DC} of 463 S cm^{-1} were investigated. The σ_{DC} values obtained in our Untreated and EG-added films, ~ 70 S cm^{-1} and ~ 500 S cm^{-1}, respectively, show a similar trend in those reported in ref. [41] Therefore, in our study the $\widetilde{\sigma}$ spectra in the terahertz region in both the Untreated and EG-added films are also analysed using the LMD model.

In the LMD model, $\widetilde{\sigma}$ spectra are expressed as follows.

$$\sigma_1 = \frac{Ne^2}{m^*} \frac{\gamma}{\omega^2 + \gamma^2}\left[1 - \frac{C}{(k_F v_F)^2}\gamma^2 + \frac{C}{(k_F v_F)^2}\gamma^{\frac{3}{2}}(3\omega)^{\frac{1}{2}}\right]$$

$$\sigma_2 = (\varepsilon_0 - \varepsilon_\infty)\omega + \frac{Ne^2}{m^*}\frac{\omega}{\omega^2 + \gamma^2}\left[1 - \left(1 - \sqrt{6}\right)\frac{C}{(k_F v_F)^2}\gamma^2 - \frac{C}{(k_F v_F)^2}\gamma^{\frac{5}{2}}\left(\frac{3}{\omega}\right)^{\frac{1}{2}}\right]$$

$$(6)$$

The degree of carrier localisation effect in each film is characterised by the parameter $\frac{C}{(k_F v_F)^2}$, where k_F is a Fermi wavenumber and v_F is a Fermi velocity. C is a constant term, which is known to be equal to 1 in conjugated polymers[34,69].

In the analyses with the LMD model, it is necessary to determine the parameters of m^*, γ and ε_∞ being consistent with those evaluated in the EG-treated film, $m^* \sim 0.49 m_0$, $\hbar\gamma \sim 0.34$ eV, and $\varepsilon_\infty \sim 2.59$ (Table 2). In the analyses of the $\widetilde{\sigma}$ spectra in the terahertz region shown in Fig. 2a, b, the ε_∞ value should be modified by adding the contribution of IR-active phonons in the MIR region to the real part of the dielectric constant in the higher energy side of the terahertz region, ε_{MIR}. Substituting $\omega = 0$ for the dielectric constant due to phonons in the third term of Eq. (5) leads to the relation $\varepsilon_{MIR} = \varepsilon_0 \sum_j \frac{f_j}{\omega_j^2}$. Using the parameter sets for phonons in the EG-treated film, $\varepsilon_{MIR} \sim 26.86$ is obtained. Therefore, the resultant ε_1 at the higher energy side of the terahertz region is 29.45 by adding ε_{MIR} to $\varepsilon_\infty \sim 2.59$. Since the N values of the Untreated and EG-added films are independently determined as shown in Table 1, the fitting parameters for the $\widetilde{\sigma}$ spectra are γ, m^*, and $\frac{C}{(k_F v_F)^2}$. Furthermore, by adding the condition to reproduce the σ_{DC} value, the fitting parameter can be reduced to two. Equation (6) shows that the new parameter $\frac{C}{(k_F v_F)^2}$ is correlated to γ. In addition, the magnitudes and spectral shapes of $\widetilde{\sigma}$ in the terahertz region depend on m^* and $\frac{C}{(k_F v_F)^2}$, respectively. Therefore, m^* and $\frac{C}{(k_F v_F)^2}$ are selected as fitting parameters. As compared to the EG-treated film, localisations of carriers should be more significant in the Untreated and EG-added films and m^* should be larger. Therefore, under the

condition of $m^* > 0.49m_0$, a set of m^* and $\frac{C}{(k_F v_F)^2}$ reproducing the $\tilde{\sigma}$ spectra in the terahertz region are searched.

The results of the fitting are shown in Fig. 5. In the Untreated film, the experimental $\tilde{\sigma}$ spectra are approximately reproduced by the fitting curves (the blue solid lines) using the LMD model. The parameters used are $m^* \sim 0.56m_0$ and $\frac{C}{(k_F v_F)^2} \sim 11.4\,\mathrm{fs}^2$, from which $h\gamma \sim 0.19$ eV is obtained. The parameter values of m^*, $\frac{C}{(k_F v_F)^2}$, and $h\gamma$ are listed in Table 2.

In the EG-added film, modifications of the $\tilde{\sigma}$ spectra from those predicted by the Drude model are not so large as compared with the case of the Untreated film and it is difficult to precisely determine m^* and $\frac{C}{(k_F v_F)^2}$. Therefore, we set $m^* = 0.52m_0 \pm 0.02m_0$ as a reasonable value, which is slightly larger than $m^* \sim 0.49m_0$ in the EG-treated film and smaller than $m^* \sim 0.56m_0$ in the Untreated film. Using this m^* value, the experimental $\tilde{\sigma}$ spectra are approximately reproduced as shown by the red solid lines in Fig. 5. The fitting parameter is $\frac{C}{(k_F v_F)^2}$, which is determined as $\sim 2.43\,\mathrm{fs}^2$. From these values of m^* and

$\frac{C}{(k_F v_F)^2}$, $h\gamma \sim 0.29$ eV is obtained. The precise parameter values of m^*, $\frac{C}{(k_F v_F)^2}$, and $h\gamma$ are also listed in Table 2.

In the Untreated film, $\frac{C}{(k_F v_F)^2}$ is larger and μ is considerably smaller than those in the EG-added film. This is reasonable since the degree of carrier localisation should be larger in the Untreated film than in the EG-added film due to the larger amount of PSS disturbing carrier transfers between neighbouring PEDOT clusters in the former. Indeed, assuming that the parameter C is equal to 1 in common, the dimensionless parameter $k_F l = (k_F v_F)/\gamma$ including the mean free path l, which gives an indication of whether the carriers are free or localised, is smaller in the Untreated film (1.03) than in the EG-added film (1.47). The value of $h\gamma$ in the Untreated film is smaller than that in the EG-treated film, which cannot be explained in a straightforward manner. This can be considered to originate from the fact that in the LMD model applied to the Untreated and EG-added films, the effective scattering rate is not determined by γ alone but is dominated by both γ and $\frac{C}{(k_F v_F)^2}$, that is, $\gamma/(k_F v_F)$ as mentioned above.

Hall effect measurements. The Hall effect originates from the Lorentz force added to the continuous flow of carriers in a magnetic field. Therefore, its observation provides evidence of the presence of delocalised carriers, which are responsible for band transport. Microscopically, when the wavevector operator **k** of an electron is coupled with the vector potential **A**, an electromotive force is generated perpendicular to both the current **I** and magnetic field **B**[70]. In other words, when the carriers exhibit free-electron-like behaviour and the wavevector **k** is well defined, the Hall coefficient R_H is related to the carrier density N_{Hall} as $R_H = 1/(eN_{Hall})$ under the condition that the inelastic scattering of carriers is negligibly small. However, when the carrier transport is dominated by a hopping conduction process, in which carriers propagate in discontinuous tunnelling processes, the Hall voltage is hardly observed. In fact, the Hall voltage detected in amorphous Si is only $\sim 1/10$ of that in crystalline Si, in which carriers exhibit band transport[71]. Therefore, in materials with finite structural disorder, such as PEDOT:PSS, observations of the Hall effect supported by the presence of free-electron-like carriers are extremely rare. Even when the Hall effect is observed, the derived Hall coefficient values should be considered with caution. The Hall effects were indeed investigated on PEDOT:PSS; however the Hall coefficients reported so far were different values with a wide range[32,72–74]. In a precise Hall effect measurement on a film on a Hall bar, the carrier density calculated from the Hall
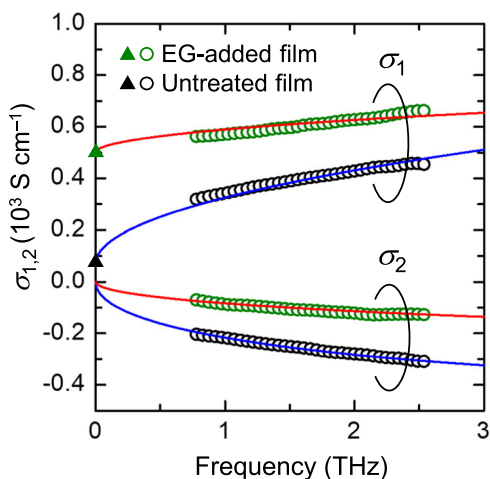

Fig. 5 Analyses of complex optical conductivity ($\tilde{\sigma}$) spectra in the terahertz region in the Untreated and EG-added films. Open circles and solid triangles show the $\tilde{\sigma}$ spectra obtained by the THz-TDS and σ_{DC}, respectively. The solid lines show the simulated spectra obtained using the LMD model.
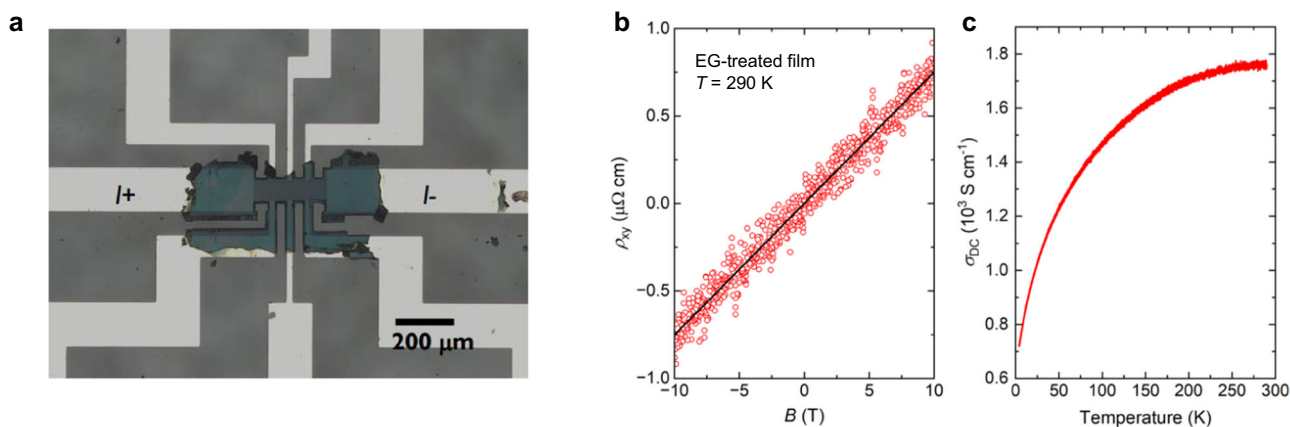

Fig. 6 Hall effect measurement of EG-treated film. a Picture of the EG-treated film on a Hall bar. **b** Hall resistivity (ρ_{xy}) along the transverse direction as a function of applied magnetic field B (red dots). The black dotted line represents a linear fitting and its slope corresponds to R_H. **c** Temperature dependence of σ_{DC} measured in the setup shown in a.

coefficient showed an unrealistic value, which was ~100 times higher than expected[72]. Therefore, it is significant to investigate the Hall effect in the PEDOT:PSS films in which the analyses of their $\tilde{\sigma}$ spectra suggest the band transport.

Herein, Hall effect measurements are performed on the EG-treated film prepared on a Hall bar, as shown in Fig. 6a. This film with a thickness of 1.2 μm exhibits σ_{DC} of 1760 S cm^{-1}, which is larger than that of the EG-treated film prepared for optical measurements (see "Methods"). To achieve high sensitivity for the Hall effect measurements, the film prepared by spin-coating is shaped into a Hall bar configuration (Fig. 6a). With a constant current flowing between the two electrodes labelled I_+ and I_- in the photograph in Fig. 6a, the Hall electromotive force is measured while the magnetic field B is varied. The transverse Hall resistivity (ρ_{xy}) derived from the Hall electromotive force is indicated by the red dots in Fig. 6b. The observed Hall effect is clearly synchronised with B. Based on the sign of the Hall electromotive force, hole carriers are responsible for electric transport. The observation of a clear Hall effect demonstrates that hole carriers are not only delocalised within each PEDOT oligomer but also between adjacent PEDOT clusters. This is consistent with the metallic response proven from the $\tilde{\sigma}$ spectra following the simple Drude model.

Next, the Hall carrier density N_{Hall} is discussed quantitatively, which is calculated from the Hall coefficient R_H using the relationship $R_H = 1/(eN_{Hall})$. At 290 K, $R_H \sim 7.5 \times 10^{-4}$ cm^3 C^{-1}, which leads to $N_{Hall} \sim 8.3 \times 10^{21}$ cm^{-3}. The N_{Hall} value is almost independent of the temperature (see Supplementary Note 6). This value is considerably larger than the carrier density $N = 8.4 \times 10^{20}$ cm^{-3} evaluated from the analysis of the $\tilde{\sigma}$ spectra with the Drude model in the EG-treated film. Previous studies have reported that in film samples of conducting polymers, the N_{Hall}/N values are in the range of 10^2 to 10^3 and rarely close to the ideal value of unity, which is ascribed to the presence of localised carriers contributing only to the hopping transport[75]. In fact, a recent model analysis of the Hall effect has shown that the ratio of N_{Hall} to the total carrier density N, N_{Hall}/N, is greater than 1 in a system where transport and hopping conduction coexist[72].

The temperature dependence of σ_{DC} should also provide important information about the nature of the carrier transport. Figure 6c shows σ_{DC} as a function of temperature, as measured using the four-point probe method on the same sample in which the Hall effect is investigated. Notably, σ_{DC} remains almost constant from 290 K to ~250 K, but decreases as the temperature decreases further, with the value at 4 K approximately half of that at 290 K. This temperature dependence of σ_{DC} is different from the typical temperature dependence observed in thermally activated or variable-range hopping conduction[72], suggesting the presence of multiple carrier transport mechanisms within the sample.

Considering this result, together with the analytical results of the $\tilde{\sigma}$ spectra and the Hall effect, the carrier transport mechanism of the PEDOT:PSS film can be understood as follows. At 294 K, the Drude response in the $\tilde{\sigma}$ spectra indicates the presence of free carriers. However, the results of the Hall effect demonstrate the presence of localised carriers. Since the $\tilde{\sigma}$ spectra are adequately reproduced by considering only the free carriers exhibiting the Drude response, it is natural to consider that carriers other than free carriers are strongly localised and hardly contribute to the optical response due to their low kinetic energies. This suggests that those carriers would be localised at defects or structural disorders due to the presence of PSS polymers near PEDOT clusters. As the temperature decreases below 250 K, σ_{DC} decreases, suggesting that all mobile carriers tend to become localised. This can be ascribed to the fact that carrier transfers between neighbouring PEDOT clusters are essential for the band

transport and the effective bandwidth is inherently not so large. Thus, the temperature dependence of σ_{DC} is considered complicated because of the temperature-induced change in the localisation effects of carriers that originally behaved as free carriers. The carriers that are strongly localised even at 294 K should not contribute to the DC conductivity, but they play an important role in the Hall effect, as pointed out above.

To verify these interpretations, the Hall effect measurement is also performed on an EG-added film with $\sigma_{DC} \sim 760$ S cm^{-1} at 290 K. In the EG-added film, R_H is evaluated to be ~2.2 × 10^{-4} cm^3 C^{-1}, which is smaller than $R_H \sim 7.5 \times 10^{-4}$ cm^3 C^{-1} in the EG-treated film. Furthermore, $N_{Hall} \sim 2.8 \times 10^{22}$ cm^{-3} calculated from R_H in the EG-added film is considerably larger than $N_{Hall} \sim 8.3 \times 10^{21}$ cm^{-3} in the EG-treated film. These comparisons demonstrate that in the EG-added film the increase of the number of localised carriers due to extrinsic factors suppresses R_H and seemingly increases the density of mobile carriers. These results support the validity of our qualitative interpretation of the Hall effect in the EG-treated film mentioned above. The details of the Hall effect in the EG-added film are reported in Supplementary Note 7. Thus, the results presented here show that quantitative information about electric transports is difficult to obtain from the Hall effect measurements on PEDOT:PSS films. The development of a theoretical model of the Hall effect that takes into account the transport mechanisms of both free and localised carriers and makes it possible to quantitatively analyse the amounts of two different types of carriers is an important subject in the future.

Because the Hall effect measurements on the EG-treated film indicate the presence of localised carriers other than free carriers responsible for the band transport, the density of free carriers is considered to be lower than $N_{EDOT} = 1/3$. Therefore, strictly, the values of m^* listed in Table 2 give their upper bound and μ listed in Table 1 give their lower bounds, and free carriers have a smaller m^* and larger μ than those values. If the net value of m^* or μ of free carriers is evaluated by other experiments, it should be possible to quantitatively determine the densities of free carriers and localised carriers, respectively. This issue is also an important task for the future.

In summary, PEDOT:PSS films with DC conductivities equal to or exceeding 1000 S cm^{-1} are fabricated by combining a multilayer spin-coating method using an EG-added aqueous solution with additional treatment of dipping the films with EG or dropping sulfuric acid onto the films. Next, the broadband complex optical conductivity spectra are evaluated, which are successfully reproduced using the Drude–Lorentz model, demonstrating that the doped hole carriers in PEDOT behave as free carriers and that band transport occurs in highly conducting PEDOT:PSS thin films. In the Hall effect measurements on an EG-treated film, the Hall electromotive force is detected, which is unambiguous evidence of the band transport. On the other hand, the carrier density derived from the Hall coefficient is considerably larger than the actual value. This is ascribed to the presence of localised carriers as well as free carriers. By the analyses of the $\tilde{\sigma}$ spectra assuming the Drude–Lorentz model, the hole mobility values, μ, were evaluated to be 7.1 (10.7) cm^2 V^{-1} s^{-1} in the EG-treated film (HS-treated film). Since a part of carriers are localised and do not contribute to the electric transport, the net μ values of free carriers responsible for the band transport are expected to be higher than the estimated values 7.1 (10.7) cm^2 V^{-1} s^{-1} in the EG-treated film (HS-treated film). The estimated high mobility values suggest that the combination of the multilayer spin-coating method and additional treatments with EG or sulfuric acid eliminates the insulating PSS polymers, which would enhance hole transfers

between neighbouring clusters and reduce defects and structural disorders responsible for localised carriers. It is an important future task to evaluate the size and distribution of PEDOT clusters in films fabricated under different conditions and to relate them with the transport mechanism. Finally, we would like to emphasize that the methodology reported here, which combines THz-TDS and reflection spectroscopy from the UV to FIR region, allows the evaluation of broadband complex optical conductivity spectra. This approach can be applied not only to PEDOT:PSS films deposited using different methods but also to various other types of conducting films. Therefore, the proposed methodology contributes to unravelling the transport mechanisms in such films and holds great potential for future research.

Methods

Preparation of PEDOT:PSS films and measurement of DC conductivity. PEDOT:PSS films are fabricated via a spin-coating method employed on a quartz substrate using the PEDOT:PSS dispersion aqueous solution (Clevios PH1000, H. C. Starck). In this method, the film thickness can be controlled by varying the substrate rotation speed. As the rotational speed decreases, the film thickness becomes thicker. At a rotation speed of 600 rpm, a PEDOT:PSS film with a thickness of ~100 nm can be produced on a quartz substrate. In the present study, to produce a thicker film, further depositions of PEDOT:PSS by additional spin-coating processes are performed on the film grown by the first spin-coating process. In that case, a thicker film of 200–250 nm is produced in each spin-coating process at the same 600 rpm rotational speed. The difference in the thickness of the films deposited by the first and second or subsequent spin-coating processes is probably due to the difference in wettability between the glass substrate and the PEDOT:PSS.

Untreated film. This film is prepared using the spin-coating method with the aforementioned PEDOT:PSS dispersion aqueous solution. Subsequently, the film is heated at 150 °C for 10 min in ambient air to remove excess moisture. This process is repeated four times to grow a film with a thickness of 800 nm; this is called the multilayer spin-coating method[38].

EG-added film. Ethylene glycol (EG, 3 wt%), a polar solvent, is added to the PEDOT:PSS dispersion aqueous solution, and a thin film with a thickness of 100 nm is prepared by a single spin-coating process using this solution. Hereafter, the EG-added solution is referred to as EG ink.

EG-treated film. Using the EG ink, a film is prepared by repeating the same spin-coating and thermal treatment process for four cycles, similar to the growth of the Untreated film. Subsequently, the film is immersed in EG for an additional 5 min, followed by a final heating step at 150 °C for 10 min to remove EG molecules. Finally, a film with a thickness of 800 nm is obtained.

HS-treated film. After a single spin-coating treatment using the EG ink, the film is heated at 150 °C for 10 min in ambient air. Subsequently, a 1:5 v/v H_2SO_4/methanol solution is drop-casted onto the film, and the sample is heated at 150 °C for 10 min after removing the H_2SO_4 by rotating the substrate at a rotation speed of 600 rpm. This process is repeated four times to grow a film with a thickness of 800 nm.

The thickness of each film is measured by using a profilometer. The error in the evaluated thickness is within ±2.5%. σ_{DC} is measured using a four-point probe method with 1.5 mm between the voltage terminals. It has been verified that thin films prepared by the same deposition method show almost identical DC conductivity and optical spectra.

Terahertz time-domain spectroscopy. In the THz-TDS[8], a mode-locked Ti: sapphire laser with a central wavelength of 800 nm (1.55 eV), repetition rate of 80 MHz, and pulse width of 30 fs is used as a light source. A (110)-oriented ZnTe emitter with a thickness of 1 mm excited by a Ti: sapphire laser pulse is adopted as the THz-pulse source. A photoconductive antenna with low-temperature-grown GaAs excited by a part of the Ti: sapphire laser pulse is used as the detector.

Owing to the high reflectivity of the films in the THz region, the light transmitted through each film is significantly weak. Considering this, an automated measurement system is introduced in which the THz electric-field waveforms of light transmitted through the PEDOT:PSS film on a quartz substrate and a quartz substrate without film are alternately measured[43]. This allows for the accurate measurement of the THz electric-field waveforms of the transmitted light by eliminating the influence of the laser source and humidity fluctuations. To derive the $\widetilde{\sigma}$ spectra of the films, the refractive index of the substrate itself is necessary and evaluated using the same measurement system. In the derivation of the $\widetilde{\sigma}$ spectra in each film, the multiple reflections (infinite) of the THz waves within the PEDOT:PSS film are considered[41,43].

Measurements of broadband optical reflectivity spectra and their analyses. Broadband reflection spectroscopy is performed on the EG- and HS-treated films, both of which have a thickness of 800 nm. The R spectra are evaluated using four different methods depending on the energy range. The R spectra in the range of 0.75–2.6 THz (0.003–0.011 eV) are calculated from the $\widetilde{\sigma}$ spectra obtained by the THz-TDS. For higher photon energies, the R spectra are directly measured. In the range of 0.012–0.5 eV, FTIR (JASCO FTIR-6100) is employed. A bolometer (Infrared Laboratories Hi Res 4.2 K Bolometer System) is used for the FIR region (0.012–0.08 eV), and a mercury cadmium telluride detector is used for the MIR region (0.08–0.5 eV). For the region of 0.011–0.012 eV, where the measurement is difficult, the data are interpolated using a straight line. For the near-infrared (NIR) to UV region (0.5–6 eV), a diffraction grating spectrometer (JASCO MSV-5200) is used. The detectors used are a PbS photovoltaic cell and a photomultiplier. Both the FTIR and diffraction grating spectrometer systems are equipped with spectroscopic microscopes, which enable the selective measurement on a clean area of the film, i.e., a square of side 400 μm and a circle of diameter 400 μm, respectively.

In both the EG- and HS-treated films, light is slightly transmitted even in the energy region below 0.8 eV where the metallic response appears; however, the transmittance is extremely low because of their thickness (800 nm). In the THz region, the transmittances of the EG- and HS-treated films are ~0.9% and 0.3%, respectively. As the frequency increases beyond the THz region, the transmittance decreases further in the MIR region and then starts increasing around 0.4 eV. The transmittances in the NIR region (0.8 eV) are 2.0% and 0.15% for the EG- and HS-treated films, respectively, remaining relatively small. In contrast, in the higher energy region of 1.1–5 eV for the EG-treated film (1.2–5 eV for the HS-treated film), the transmittance becomes large; a slight periodic oscillation is evident in the R spectrum, which is attributed to the interference between the reflected light from the film and the reflected light from the substrate after the light is transmitted through the film. However, the amplitudes of these oscillations are limited, suggesting that the effect of transmission on the measured R value can be neglected. Based on these features, the obtained R spectra are

considered accurate in the range of 0.012–6 eV for both the EG- and HS-treated films.

To apply the KKT to the obtained broadband R spectra, the R data outside the measured range are extrapolated as follows. The Hagen–Rubens rule[76] is used for extrapolation on the low-frequency side. This is reasonable since σ_1 evaluated by the THz-TDS is almost constant in the THz region and is in good agreement with σ_{DC} for both the EG- and HS-treated films. Above the higher energy bound of the measured range, the strong electronic (π–π^*) transitions are known to exist[77], which should be excluded from our analyses based on the Drude model. Considering this, R above 3.1 eV (3.8 eV) is set as a constant equal to the value at 3.1 eV (3.8 eV) in the EG-treated (HS-treated) film. R above 100 eV is assumed proportional to ω^{-4}, where ω is the angular frequency.

Hall effect measurements. To measure the Hall effect, a Hall bar is fabricated by patterning electrodes on a glass substrate. Specifically, Cr (8 nm) and Au (20 nm) electrodes are deposited on a 0.7-mm-thick EAGLE XG glass substrate in combination with a standard two-layer lift-off process to form channel length L and width W of 72 μm and 240 μm, respectively. After fabricating the electrodes, the device is cleaned in an ozone cleaner before coating. EG-treated films are prepared on Hall bars using the same method as that used for the optical measurements. The thickness of the EG-treated film, measured using a profilometer, is 1.2 μm. The film is etched using an yttrium aluminium garnet laser to match the shape of the Hall bar, making it possible to accurately measure the local potential of the probe along the channel. After the deposition, the device is encapsulated with CYTOP 809 M (AGC Chemicals).

σ_{DC} of the EG-treated film prepared on the Hall bar is 1760 S cm^{-1} at 290 K, which is higher than that of the film prepared on the quartz substrate for optical measurements. Possible reasons for the enhanced conductivity of the PEDOT:PSS film may be that PSS exclusion is more likely to occur on the glass substrate with electrodes and that the quality of the film itself is improved. The latter may be related to the fact that films tend to grow better on the electrodes. Hall effect measurements are performed at 250 K and 200 K as well as 290 K in a helium gas-exchange cryostat with a superconducting magnet. The Hall resistivity (ρ_{xy}) along the transverse direction is measured using a lock-in detection technique. An AC excitation current of 5 μA is applied under an external and perpendicular magnetic field B with a slow sweeping rate of 0.01 T s^{-1}.

Data availability

The data that support the plots within this paper and other findings of this study are available from the corresponding author upon reasonable request.

References

1. Janata, J. & Josowicz, M. Conducting polymers in electronic chemical sensors. *Nat. Mater.* **2**, 19–24 (2003).
2. Seo, S. et al. An ultra-thin, un-doped NiO hole transporting layer of highly efficient (16.4%) organic–inorganic hybrid perovskite solar cells. *Nanoscale* **8**, 11403–11412 (2016).
3. He, H. et al. A self-powered electronic-skin for real-time perspiration analysis and application in motion state monitoring. *J. Mater. Chem. C* **6**, 9624–9630 (2018).
4. Afzali, A., Dimitrakopoulos, C. D. & Breen, T. L. High-performance, solution-processed organic thin film transistors from a novel pentacene precursor. *J. Am. Chem. Soc.* **124**, 8812–8813 (2002).
5. Levermore, P. A., Jin, R., Wang, X., De Mello, J. C. & Bradley, D. D. C. Organic light-emitting diodes based on poly (9,9-dioctylfluorene-co-bithiophene) (F8T2). *Adv. Funct. Mater.* **19**, 950–975 (2009).
6. Li, Q. et al. Flexible high-temperature dielectric materials from polymer nanocomposites. *Nature* **523**, 576–579 (2015).
7. Wang, J. et al. Conducting-polymer-based materials for electrochemical energy conversion and storage. *Adv. Mater.* **29**, 1703044 (2017).
8. Wang, C., Zhang, X., Dong, H., Chen, X. & Hu, W. Organic field-effect transistors: challenges and emerging opportunities in high-mobility and low-energy-consumption organic field-effect transistors. *Adv. Energy Mater.* **10**, 2070126 (2020).
9. Riede, M., Spoltore, D. & Leo, K. Organic solar cells—the path to commercial success. *Adv. Energy Mater.* **11**, 2002653 (2021).
10. Shirakawa, H., Louis, E. J., MacDiarmid, A. G., Chiang, C. K. & Heeger, A. J. Synthesis of electrically conducting organic polymers: halogen derivatives of polyacetylene, (CH)$_x$. *J. Chem. Soc. Chem. Commun.* **16**, 578–580 (1977).
11. Ivory, D. M. et al. Highly conducting charge-transfer complexes of poly(p-phenylene). *J. Chem. Phys.* **71**, 1506–1507 (1979).
12. Street, G. B. et al. Preparation and characterization of neutral and oxidized polypyrrole films. *Mol. Cryst. Liq. Cryst.* **83**, 253–264 (1982).
13. Yoshino, K., Nakao, K., Onoda, M. & Sugimoto, R. Novel doping effect of conducting polymer gel. *Jpn. J. Appl. Phys* **28**, L682 (1989).
14. Tsukamoto, J., Takahashi, A. & Kawasaki, K. Structure and electrical properties of polyacetylene yielding a conductivity of 10^5 S/cm. *Jpn. J. Appl. Phys.* **29**, 125–130 (1990).
15. Kaur, G., Adhikari, R., Cass, P., Bown, M. & Gunatillake, P. Electrically conductive polymers and composites for biomedical application. *RSC Adv.* **5**, 37553–37567 (2015).
16. Nezakati, T., Seifalian, A., Tan, A. & Seifalia, A. M. Conductive polymers: opportunities and challenges in biomedical applications. *Chem. Rev.* **118**, 6766–6843 (2018).
17. Sumdani, M. G., Islam, M. R., Yahaya, A. N. A. & Safie, S. I. Recent advancements in synthesis, properties, and applications of conductive polymers for electrochemical energy storage devices: a review. *Polym. Eng. Sci.* **62**, 269–303 (2022).
18. Zhao, Q., Jamal, R., Zhang, L., Wang, M. & Abdiryim, T. The structure and properties of PEDOT synthesized by template-free solution method. *Nanoscale Res. Lett.* **9**, 557 (2014).
19. Yamashita, Y. et al. Supramolecular cocrystals built through redox-triggered ion intercalation in π-conjugated polymers. *Commun. Mater.* **2**, 1–9 (2021).
20. Sonmez, G. Polymeric electrochromics. *Chem. Commun.* **42**, 5251–5259 (2005).
21. Bischak, C. G. et al. A reversible structural phase transition by electrochemically-driven ion injection into a conjugated polymer. *J. Am. Chem. Soc.* **142**, 7434–7442 (2020).
22. Paulsen, B. et al. Time-resolved structural kinetics of an organic mixed ionic–electronic conductor. *Adv. Mater.* **32**, 2003404 (2020).
23. Wu, X. et al. Enhancing the electrochemical doping efficiency in diketopyrrolopyrrole-based polymer for organic electrochemical transistors. *Adv. Electron. Mater.* **7**, 2000701 (2021).
24. Rebetez, G., Bardagot, O., Affolter, J., Réhault, J. & Banerji, N. What drives the kinetics and doping level in the electrochemical reactions of PEDOT:PSS? *Adv. Funct. Mater.* **32**, 2105821 (2022).
25. De Kok, M. M. et al. Modification of PEDOT:PSS as hole injection layer in polymer LEDs. *Phys. Stat. Solidi. (A)* **201**, 1342–1359 (2004).
26. Dubey, N. & Leclerc, M. Conducting polymers: efficient thermoelectric materials. *J. Polym. Sci. B Polym. Phys.* **49**, 467–475 (2011).
27. Kim, S. et al. Influence of PEDOT:PSS crystallinity and composition on electrochemical transistor performance and long-term stability. *Nat. Commun.* **9**, 3858 (2018).
28. Takano, T., Masunaga, H., Fujiwara, A., Okuzaki, H. & Sasaki, T. PEDOT nanocrystal in highly conductive PEDOT:PSS polymer films. *Macromolecules* **45**, 3859–3865 (2012).
29. Horii, T., Li, Y., Mori, Y. & Okuzaki, H. Correlation between the hierarchical structure and electrical conductivity of PEDOT/PSS. *Polym. J.* **47**, 695–699 (2015).
30. Lang, U., Muller, E., Naujoks, N. & Dual, J. Microscopical investigations of PEDOT:PSS thin films. *Adv. Funct. Mater.* **19**, 1215–1220 (2009).
31. Kim, Y. H. et al. Highly conductive PEDOT:PSS electrode with optimized solvent and thermal post-treatment for ITO-free organic solar cells. *Adv. Funct. Mater.* **21**, 1076–1081 (2011).
32. Lin, Y., Ni, W. & Lee, J. Effect of incorporation of ethylene glycol into PEDOT:PSS on electron phonon coupling and conductivity. *J. Appl. Phys.* **117**, 215501 (2015).

33. Palumbiny, C. et al. The crystallization of PEDOT:PSS polymeric electrodes probed in situ during printing. *Adv. Mater.* **27**, 3391–3397 (2015).

34. Kim, N. et al. Role of interchain coupling in the metallic state of conducting polymers. *Phys. Rev. Lett.* **109**, 106405 (2012).

35. Ouyang, J. et al. On the mechanism of conductivity enhancement in poly(3,4-ethylenedioxythiophene):poly(styrene sulfonate) film through solvent treatment. *Polymer* **45**, 8443–8450 (2004).

36. Kim, N. et al. Highly conductive PEDOT:PSS nanofibrils induced by solution-processed crystallization. *Adv. Mater.* **26**, 2268–2272 (2014).

37. He, S., Mukaida, M., Kirihara, K., Lyu, L. & Wei, Q. Reversible protonic doping in poly(3,4-ethylenedioxythiophene). *Polymers* **10**, 1065 (2018).

38. Kim, N. et al. Highly conductive all-plastic electrodes fabricated using a novel chemically controlled transfer-printing method. *Adv. Mater.* **27**, 2317–2323 (2015).

39. Kumar, S., Kurra, N. & Alshareef, H. Enhanced high temperature thermoelectric response of sulphuric acid treated conducting polymer thin films. *J. Mater. Chem. C* **4**, 215–221 (2016).

40. Yano, H., Kudo, K., Marumo, K. & Okuzaki, H. Fully soluble self-doped poly(3,4-ethylenedioxythiophene) with an electrical conductivity greater than 1000 S cm^{-1}. *Sci. Adv.* **5**, eaav9492 (2019).

41. Yamashita, M., Otani, C., Shimizu, M. & Okuzaki, H. Effect of solvent on carrier transport in poly(3,4-ethylenedioxythiophene)/ poly(4-styrenesulfonate) studied by terahertz and infrared-ultraviolet spectroscopy. *Appl. Phys. Lett.* **99**, 143307 (2011).

42. Smith, N. V. Classical generalization of the Drude formula for the optical conductivity. *Phys. Rev. B* **64**, 155106 (2001).

43. Yan, F., Parrott, E., Ung, B. & MacPherson, E. Solvent doping of PEDOT/PSS: effect on terahertz optoelectronic properties and utilization in terahertz devices. *J. Phys. Chem. C* **119**, 6813–6818 (2015).

44. Du, Y. et al. Dielectric properties of DMSO-Doped-PEDOT:PSS at THz frequencies. *Phys. Status Solidi B* **255**, 1700547 (2018).

45. Fratini, S., Ciuchi, S. & Mayou, D. Phenomenological model for charge dynamics and optical response of disordered systems: application to organic semiconductors. *Phys. Rev. B* **89**, 235201 (2014).

46. Kim, Y., Kim, Y. & Kim, J. Highly conductive PEDOT:PSS thin films with two-dimensional lamellar stacked multi-layers. *Nanomaterials* **10**, 10 (2020).

47. Hosseini, E., Ozhukil Kollath, V. & Karan, K. The key mechanism of conductivity in PEDOT:PSS thin films exposed by anomalous conduction behaviour upon solvent-doping and sulfuric acid post-treatment. *J. Mater. Chem. C.* **8**, 3982–3990 (2020).

48. Pustogow, A. et al. Quantum spin liquids unveil the genuine Mott state. *Nat. Mater.* **17**, 773–777 (2018).

49. Yada, H. et al. Evaluating intrinsic mobility from transient terahertz conductivity spectra of microcrystal samples of organic molecular semiconductors. *Appl. Phys. Lett.* **115**, 143301 (2019).

50. Han, Y. et al. Scattering mechanism of hole carriers in organic molecular semiconductors deduced from analyses of terahertz absorption spectra using Drude-Anderson model. *Appl. Phys. Lett.* **120**, 053302 (2022).

51. Hwang, J., Tanner, D. B., Schwendeman, I. & Reynolds, J. R. Optical properties of nondegenerate ground-state polymers: Three dioxythiophene-based conjugated polymers. *Phys. Rev. B* **67**, 115205 (2003).

52. Hwang, J. et al. In situ measurements of the optical absorption of dioxythiophene-based conjugated polymers. *Phys. Rev. B* **83**, 195121 (2011).

53. Tounakti, C., Decorse, P. & Kouki, F. Relationship between enhancement of PEDOT:PSS conductivity by solvent treatment and PSS chain reorganization. *J. Polym. Sci.* **61**, 582–603 (2023).

54. Yemata, T. A. et al. Modulation of the doping level of PEDOT:PSS film by treatment with hydrazine to improve the Seebeck coefficient. *RSC Adv.* **10**, 1786–1792 (2020).

55. Atoyo, J., Burton, M. R., Mcgettrick, J. & Carnie, M. J. Enhanced electrical conductivity and Seebeck coefficient in PEDOT:PSS via a two-step ionic liquid and NaBH$_4$ treatment for organic thermoelectrics. *Polymers* **12**, 559 (2020).

56. DeLongchamp, D. M. et al. Influence of a water rinse on the structure and properties of poly(3,4-ethylene dioxythiophene):Poly(styrene sulfonate) films. *Langmuir* **21**, 11480–11483 (2005).

57. Zotti, G. et al. Electrochemical and XPS studies toward the role of monomeric and polymeric sulfonate counterions in the synthesis, composition, and properties of poly(3,4-ethylenedioxythiophene). *Macromolecules* **36**, 3337–3344 (2003).

58. Crispin, X. et al. Conductivity, morphology, interfacial chemistry, and stability of Poly (3, 4-ethylene dioxythiophene)–Poly(styrene sulfonate): a Photoelectron Spectroscopy. *Study. J. Polym. Sci. B Polym. Phys.* **41**, 2561–2583 (2003).

59. Kim, D. & Zozoulenko, I. Why is pristine PEDOT oxidized to 33%? A Density functional theory study of oxidative polymerization mechanism. *J. Phys. Chem. B* **123**, 5160–5167 (2019).

60. Ouyang, L., Musumeci, C., Jafari, M. J. & Ederth, T. Imaging the phase separation between PEDOT and polyelectrolytes during processing of highly conductive PEDOT:PSS films. *ACS Appl. Mater. Interfaces* **7**, 19764–19773 (2015).

61. Meng, W. et al. Conductivity enhancement of PEDOT:PSS films via phosphoric acid treatment for flexible all-plastic solar cells. *ACS Appl. Mater. Interfaces* **7**, 14089–14094 (2015).

62. Kim, Y., Cho, W., Kim, Y., Cho, H. & Kim, J. Electrical characteristics of heterogeneous polymer layers in PEDOT:PSS. *films. J. Mater. Chem. C* **6**, 8906–8913 (2018).

63. Asada, K. et al. Ultrafast control of electronic states by a terahertz electric field pulse in the quasi-one-dimensional organic ferroelectric (TMTTF)$_2$PF$_6$. *Phys. Rev. B* **104**, 195148 (2021).

64. Kudryavtsev, O. S. et al. Fano-type effect in hydrogen-terminated pure nanodiamond. *Nano Lett.* **22**, 2589–2594 (2022).

65. Rivnay, J. et al. Structural control of mixed ionic and electronic transport in conducting polymers. *Nat. Commun.* **7**, 11287 (2016).

66. Cai, H. et al. Intrinsic ambipolar transport for the traditional conducting or hole transport ionic blend polymer PEDOT:PSS. *Polymer* **180**, 121732 (2019).

67. Chen, S. et al. On the anomalous optical conductivity dispersion of electrically conducting polymers: ultra-wide spectral range ellipsometry combined with a Drude-Lorentz. *model. J. Mater. Chem. C* **7**, 4350–4362 (2019).

68. Kong, M., Garriga, M., Sebasti, J. & Alonso, M. I. Advanced optical characterization of PEDOT:PSS by combining spectroscopic ellipsometry and Raman scattering. *ACS Omega* **7**, 39429–39436 (2022).

69. Mott, N. F. & Kaveh, M. Metal-insulator transitions in non-crystalline systems. *Adv. Phys.* **34**, 329–401 (1985).

70. Fukuyama, H., Ebisawa, H. & Wada, Y. Theory of Hall effect. I- nearly free electron. *Prog. Theor. Phys.* **42**, 494–511 (1969).

71. Arnold, E. & Shannon, J. Anomalous Hall effect and carrier transport in bandtails at the Si-SiO$_2$ interface. *Solid State Commun.* **18**, 1153–1156 (1976).

72. Kang, K. et al. 2D coherent charge transport in highly ordered conducting polymers doped by solid state diffusion. *Nat. Mater.* **15**, 896–902 (2016).

73. Dauzon, E. et al. Conducting and stretchable PEDOT:PSS electrodes: role of additives on self-assembly, morphology, and transport. *ACS Appl. Mater. Interfaces* **11**, 17570–17582 (2019).

74. Sato, R., Wasai, Y., Izumi, Y., Ueno, K. & Shirai, H. Influence of effective mass on carrier concentration for PEDOT:PSS and S-PEDOT thin films studied by ellipsometry and Hall measurement. *J. Phys. Chem. C* **127**, 13196–13206 (2023).

75. Yi, H. T., Gartstein, Y. N. & Podzorov, V. Charge carrier coherence and Hall effect in organic semiconductors. *Sci. Rep.* **6**, 23650 (2016).

76. Hagen, E. & Rubens, H. Über Beziehungen des Reflexions- und Emissionsvermögens der Metalle zu ihrem elektrischen Leitvermögen. *Ann. Phys.* **11**, 873–901 (1903).

77. Pettersson, L. A. A., Ghosh, S. & Inganäs, O. Optical anisotropy in thin films of poly(3,4-ethylenedioxythiophene)-poly(4-styrenesulfonate). *Org. Electron.* **3**, 143–148 (2002).

Author contributions

Q.W. and M.M. provided the thin film samples of PEDOT:PSS. T.M. and H.O. constructed the infrared reflection spectroscopy system. N.T., N.K., T.M., Y.H. and R.I. constructed the THz-TDS system. A part of the THz-TDS measurements were done with the help of M.O. and Y.T. Z.G., T.S. and N.T. performed the optical measurements. T.S., Z.G., N.T. and T.M. analysed the optical spectra. N.K., S.W. and J.T. performed the Hall effect measurements. H.O. coordinated the study. Z.G., T.S., S.W. and H.O. wrote the paper with inputs from all the authors.

Additional information

Supplementary information The online version contains supplementary material available at https://doi.org/10.1038/s43246-024-00451-1.

Correspondence and requests for materials should be addressed to Hiroshi Okamoto.

Peer review information *Communications Materials* thanks Sergi Riera Galindo, Kunal Karan and the other, anonymous, reviewer(s) for their contribution to the peer review of this work. Primary Handling Editors: Jet-Sing Lee. A peer review file is available.

Reprints and permission information is available at http://www.nature.com/reprints

Publisher's note Springer Nature remains neutral with regard to jurisdictional claims in published maps and institutional affiliations.